

Beyond Flicker: Detecting Kinematic Inconsistencies for Generalizable Deepfake Video Detection

Alejandro Cobo ^{*1}, Roberto Valle¹, José Miguel Buenaposada², Luis Baumela¹

¹Universidad Politécnica de Madrid, Campus de Montegancedo s/n, Boadilla del Monte, 28660, Madrid, Spain

²Universidad Rey Juan Carlos, Calle Tulipán s/n, Móstoles, 28933, Madrid, Spain

Abstract. Generalizing deepfake detection to unseen manipulations remains a key challenge. A recent approach to tackle this issue is to train a network with pristine face images that have been manipulated with hand-crafted artifacts to extract more generalizable clues. While effective for static images, extending this to the video domain is an open issue. Existing methods model temporal artifacts as frame-to-frame instabilities, overlooking a key vulnerability: the violation of natural motion dependencies between different facial regions. In this paper, we propose a synthetic video generation method that creates training data with subtle kinematic inconsistencies. We train an autoencoder to decompose facial landmark configurations into motion bases. By manipulating these bases, we selectively break the natural correlations in facial movements and introduce these artifacts into pristine videos via face morphing. A network trained on our data learns to spot these sophisticated biomechanical flaws, achieving state-of-the-art generalization results on several popular benchmarks.

1 Introduction

Deepfakes refer to audiovisual media of human subjects whose content has been manipulated or entirely generated by artificial methods. Although these techniques are useful in scenarios such as filmmaking or social media applications, they can also be exploited for malicious purposes, including spreading misinformation and identity theft.

Consequently, as deepfake generation methods grow in sophistication, so does the need for advanced detection systems that can reliably identify manipulated media, particularly from unseen generation methods. A successful approach to improve generalization is the use of pseudo-fake generation techniques [1, 4, 16, 17, 23, 29, 33, 39], in which fake samples are generated from pristine data to train a predictive model. This allows for a higher controllability of the data presented to the model, including samples that are very similar to their pristine counterparts, which forces the network to extract more informative representations to distinguish between real and manipulated faces.

Present pseudo-fake deepfake detection approaches mainly focus on detecting *spatial artifacts* such as blending boundaries and texture inconsistencies [17, 29] and *temporal artifacts* associated with the digital fingerprint of different video sources [33] and the flicker or drift of individ-

ual facial features over time [1, 23, 39]. However, they do not investigate the violation of natural motion dependencies between different facial parts. For example, the fake in Fig. 1 would go unnoticed since there is no temporal drift, but a very subtle uncorrelation between the movement of the eyebrow and the eyelid. We argue that modern deepfake generation methods are progressively introducing less obvious temporal artifacts, and present pseudo-fake approaches could be rendered insufficient.

Real human faces are not collections of independent parts; they are complex systems governed by an underlying musculature and skeletal structure. The movement of one part is biomechanically linked to that of others, creating a set of natural correlated motion patterns. Deepfake models, especially those that might learn to render different facial parts in a semi-independent manner, can fail to reproduce these complex correlations. This results in motions without temporal artifacts that look plausible in isolation but are subtly wrong in their relationship to each other.

Hence, in this paper, we propose a new data-driven methodology to synthesize subtle temporal artifacts. Our approach is built on a novel generative model of facial kinematics, which we use within a flexible synthesis framework to create a diverse range of subtle motion inconsistencies. This allows us to train detectors that are more sensitive to the sophisticated forgeries produced by modern deepfake models.

^{*}Corresponding author: alejandro.cobo@upm.es

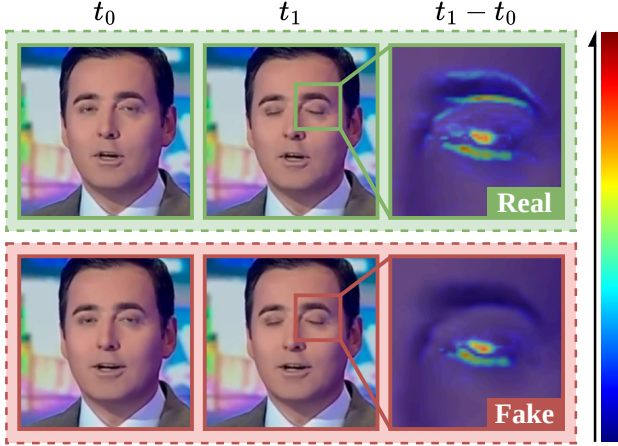


Figure 1. Example of temporal artifacts introduced by a deepfake generation method [30]. It fails to accurately replicate the correlation between eyebrow and eyelid movements observed during eye closure in the original video.

In summary, our contributions can be listed as follows:

1. A data-driven generator for facial motion artifacts. We propose a generative model, based on an autoencoder architecture, that learns a structured representation of facial kinematics.
2. A flexible synthesis pipeline for non-rigid temporal forgery. We introduce a synthesis process that adapts established face warping techniques for a new purpose: applying targeted, non-rigid temporal artifacts driven by our learned motion generator. This approach goes beyond previous methods that have focused on more holistic, face-wide transformations, allowing for a new level of detail and realism in the synthesized artifacts.
3. A new state-of-the-art in generalizable deepfake video detection. We empirically demonstrate that a hybrid training strategy, combining existing spatial pseudo-fakes with our proposed temporal artifacts outperforms previous approaches on multiple leading benchmarks.

2 Related work

Deepfake detection. Early works in deepfake detection focused on extracting image-level clues, either in the RGB space [27] or in the frequency space [25], but do not generalize well to unseen manipulation techniques. Some methods expanded to video inputs to take advantage of more informative spatiotemporal features [5, 11, 33, 34, 41]. Moreover, since spatial artifacts usually dominate deepfake videos, it is not easy for the model to correctly learn to identify temporal clues [41]. To improve generalization towards different deepfake generation methods, many works leverage techniques such as contrastive learning [10, 16], atten-

tion mechanisms [14, 40] or self-supervision [4, 11].

Recent approaches focus on adapting large foundational models for the deepfake detection task [1, 12, 19, 28, 38, 39] and the usage of multi-task frameworks that include auxiliary tasks related to deepfake detection [3, 5, 23]. However, generalization to unseen manipulation methods requires not only an appropriate model architecture, but most importantly, the correct data to train the network, as it is crucial for the model to be guided toward extracting the most relevant features. Thus, we propose a new framework to generate synthetic videos that is independent of any model architecture and can be combined with existing solutions.

Pseudo-fake generation. A popular approach to improve generalization is to leverage a data augmentation technique termed pseudo-fake generation, where manipulated examples are generated from pristine data as the model trains. By training with real samples slightly modified with artifacts common to most deepfake generation methods, we can guide the network to extract more general features and avoid overfitting to specific clues introduced by particular deepfake generation methods, which yields better generalization results.

The first pseudo-fake generation methods simulated face swap by blending two images of the same subject in different scenarios [17], and this was later improved by using two slightly different copies of the same image (SBI) [29]. These methods work well for detecting face swap-style manipulations, but underperform when exposed to other forgery types, such as face reenactment, or methods that leave less obvious blending traces (see Tab. 2).

This has motivated subsequent research to explore the generalization of this idea to video sequences [1, 23, 33, 39]. *Altfreezing* [33] performs clip-level blending (CBI), where faces in two video clips are blended frame-by-frame. *FakeSTormer* [23] and *DeepShield* [1] apply the SBI pipeline jointly to all frames in a video clip. *VB* [39] applies global affine transformations localized to inner facial regions, and constructs a sequence of independently manipulated frames. However, in CBI [33], substantial unrealistic artifacts can be introduced if the motion portrayed in the two clips differs greatly. In the case of [1, 23, 39], the complex nature of correlated movements between facial regions is not considered, as this is approximated by a simple face-wide blending procedure. It is also important to note that temporal artifacts in deepfake videos include not only extra movements not present in the original sequence, but also the lack of correlation between the motion of different facial components, as shown in Fig. 1. Hence, we propose to generate temporal artifacts following a data-driven approach, as these inconsistencies cannot be modeled with analytical approximations.

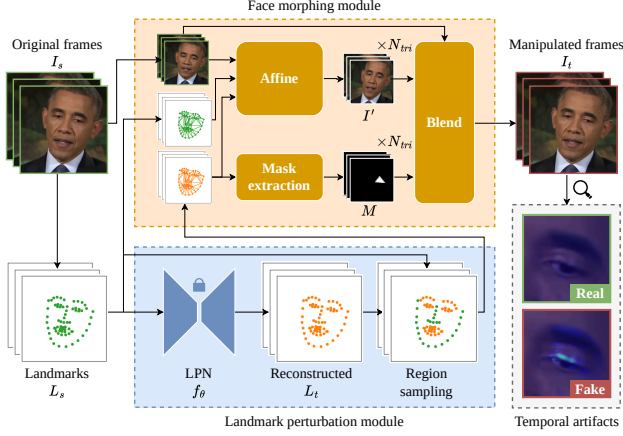


Figure 2. Overview of our method. We leverage a pretrained Landmark Perturbation Network (LPN) that is able to introduce subtle temporal artifacts to landmark sequences extracted from real videos. We then introduce these artifacts to the original frames by modulating facial regions to match the movement of the manipulated landmark sequence. The resulting frames contain generic temporal clues that can be used to train deepfake video detection models.

3 Method

Fig. 2 shows an overview of our pseudo-fake generation framework, called Kinematic Model for facial motion Inconsistencies (KiMol). First, we extract landmark annotations from a frame sequence and leverage a pretrained Landmark Perturbation Network (LPN) to introduce realistic temporal artifacts to the landmark sequence. This yields a new sequence that closely resembles the original, but with added subtle differences. Then, we apply a face morphing pipeline to distort facial regions in the original frames to follow the movement portrayed in the reconstructed landmarks, resulting in a pseudo-fake video containing temporal artifacts. In the following sections, we explain in more detail the various parts of our method.

3.1 Problem formulation

We aim to generate pseudo-fake videos by introducing subtle temporal artifacts to pristine frames sequences. To do so, we first simplify the definition of facial movement to a sequence of N_{lnd} sparse facial landmarks [9], $L \in \mathbb{R}^{T \times N_{lnd} \times 2}$, where T is the number of frames in a video clip. We define the facial movement portrayed in the sequence, $\delta L \in \mathbb{R}^{(T-1) \times N_{lnd} \times 2}$, as the difference between landmark coordinates in consecutive frames:

$$\delta L = \{L^{i+1} - L^i\}_{i=1}^{T-1}. \quad (1)$$

Therefore, given two aligned landmark sequences, L_R and L_F , portraying the same scene in real and fake videos,

respectively, we can calculate the temporal artifacts introduced by a manipulation method as:

$$\Delta_t = \delta L_F - \delta L_R. \quad (2)$$

Since facial movements involve an extraordinarily complex interaction among different muscles and organs, we hypothesize that Δ_t cannot be accurately approximated by analytical means, such as global affine transformations, especially considering the rapid development of deepfake generation techniques that may account for temporal consistency. This is also shown in Fig. 5a, which depicts the complex correlation between the landmarks in Δ_t in a deepfake dataset [13]. Therefore, we propose to approximate these temporal artifacts with a neural network, $f_\theta(\cdot)$, as $\Delta_t \approx \delta f_\theta(L_R) - \delta L_R$ in a data-driven approach.

3.2 Landmark Perturbation Network

To simulate the temporal artifacts found in deepfake videos, we take advantage of a neural network $f_\theta(\cdot)$ trained to reconstruct landmark sequences (see Fig. 3). Building upon prior methods that utilize face-wide blending operations [1, 23, 33, 39], our work introduces a more flexible approach. We focus on generating a diverse set of localized and non-rigid transformations to provide a richer set of training clues. For this, the network is trained to decompose facial landmark configurations into a series of k learnable deformation bases $B \in \mathbb{R}^{k \times d}$, where d is the size of the latent space. The encoder \mathcal{E} takes the input landmark sequence $L \in \mathbb{R}^{T \times N_{lnd} \times 2}$ and outputs a matrix $W \in \mathbb{R}^{T \times k}$. Each row in W contains the weights for all deformation bases that better approximate the input landmark configuration for a particular time step. The input of the decoder \mathcal{D} , $\mathbf{x}_D \in \mathbb{R}^{T \times d}$ is the weighted sum of all deformation bases for each time step $\mathbf{x}_D = WB$. The decoder then reconstructs the original sequence relying only on this weighted sum of deformation bases.

In practice, we implement $f_\theta(\cdot)$ as a transformer network [31], due to its superior performance on time series tasks. Landmark coordinates for each time step are projected into tokens $\mathbf{x}_E \in \mathbb{R}^{T \times d}$, and a masked attention mechanism is used to improve the temporal consistency of the output sequence.

The reconstruction loss is defined as the squared euclidean distance between the input L and reconstructed $\hat{L} = f_\theta(L)$ landmark sequences:

$$\mathcal{L}_{rec} = \frac{1}{T \cdot N_{lnd}} \sum_{i=1}^T \sum_{j=1}^{N_{lnd}} \lambda_j \|\hat{L}^i(j) - L^i(j)\|_2^2, \quad (3)$$

where λ_j denotes the weight of the j -th facial landmark in the loss calculation. We assign a higher weight value to non-rigid facial regions (i.e., eyes and mouth).

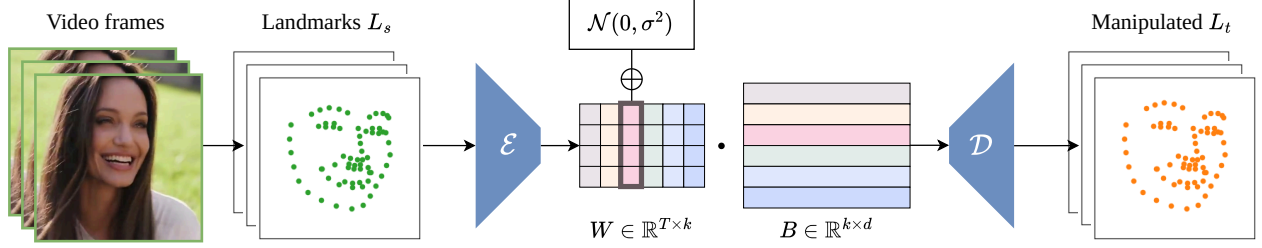


Figure 3. Overview of the Landmark Perturbation Network. The encoder \mathcal{E} generates a list of weights (W) for each time step, and the decoder \mathcal{D} reconstructs the input sequence from a weighted sum of k learnable deformation bases (B). In inference time, we generate temporal artifacts by randomly selecting a column in W and adding subtle Gaussian noise to the predicted weights. Since each deformation basis is responsible for different components in the reconstruction of the face, our approach lets us generate a diverse set of semantically meaningful artifacts.

Since the landmark configuration between consecutive time steps in real videos does not change significantly, we want the weights predicted by the encoder to also reflect this fact. For this, we add a regularization term to the loss function to minimize the distance between weights for consecutive time steps:

$$\mathcal{L}_{reg} = \frac{1}{(T-1) \cdot k} \sum_{i=1}^{T-1} \sum_{j=1}^k \|W^{i+1}(j) - W^i(j)\|_2^2. \quad (4)$$

The final loss function is the weighted sum of both components: $\mathcal{L} = \mathcal{L}_{rec} + \lambda_{reg} \cdot \mathcal{L}_{reg}$, where λ_{reg} is the weight of the regularization term. For our experiments, we set $\lambda_{reg} = 0.01$.

We use the CelebV-HQ dataset [42] to train the network, where we extract landmark annotations with the SPIGA detector [24], for a total of 34,060 landmark sequences. Once trained, we can generate a wide variety of temporal artifacts by introducing subtle noise to the weights predicted by the encoder for a particular deformation basis. For this, we randomly choose one column in W following a uniform distribution $U\{1, \dots, k\}$, and add Gaussian noise $\mathcal{N}(0, \sigma^2)$, sampled independently for each time step, to the values of the chosen column. This procedure introduces slight variations to a particular deformation basis, which modifies one aspect of the reconstructed face in the temporal direction (see Fig. 4). It is possible to generate more subtle or prominent artifacts by adjusting the noise variance σ^2 .

Furthermore, as shown in Fig. 2, we also perform a random sampling of face components to generate manipulated sequences. First, we sample a random number of face regions from the inner part of the face (i.e., eyebrows, eyes, nose, mouth), and only modify the landmarks from the selected regions, keeping the rest the same as the original sequence. This procedure is independent of the perturbations generated by the network and further improves the variety of samples generated by our method.

Algorithm 1 Face morphing algorithm.

Require: Source frames I_s , source landmarks L_s , target landmarks L_t , Delaunay triangulation \mathcal{F}

```

1:  $I_t \leftarrow I_s$ 
2: for  $i = 1, \dots, T$  do
3:   for all  $f \in \mathcal{F}$  do
4:      $\mathbf{x}_s \leftarrow \{L_s^i(j) \mid j \in f\}$ 
5:      $\mathbf{x}_t \leftarrow \{L_t^i(j) \mid j \in f\}$ 
6:      $I'_f \leftarrow \text{Affine}(I_s^i, \mathbf{x}_s, \mathbf{x}_t)$ 
7:      $M_f \leftarrow \text{MaskExtraction}(\mathbf{x}_t)$ 
8:      $I_t^i \leftarrow I_t^i \odot (1 - M_f) + I'_f \odot M_f$ 
9: return  $I_t$ 

```

Guided sampling of training data. We have observed that, to effectively train the network to model rapid movements (e.g., blinks, quick mouth movements, etc.), we must pay special attention to the sampling procedure of training data. Since the temporal window of this type of movements is very small, if we naively sample random clips of length T from landmark sequences following a uniform distribution, the network may be prone to ignore these movements, as they are statistically rare. To solve this, for each sequence, we sample clips following a Gaussian distribution centered around the time step t with the largest non-rigid movements:

$$\max_t \sum_{j \in \mathcal{J}} \|\delta L^t(j)\|_1, \text{ such that } \mathcal{J} = \{\text{eyes}, \text{mouth}\}. \quad (5)$$

3.3 Face morphing

After obtaining a sequence of landmarks generated by the LPN, our next goal is to introduce the underlying temporal artifacts into the video frames. To do so, we leverage a face morphing algorithm that modulates facial regions to match their corresponding positions in the target landmark sequence (see Algorithm 1).

In particular, the input consists of a sequence of source frames $I_s \in \mathbb{R}^{T \times H \times W \times C}$, source landmarks $L_s \in \mathbb{R}^{T \times N_{ld} \times 2}$ and target landmarks $L_t \in \mathbb{R}^{T \times N_{ld} \times 2}$, and the output is the modified frame sequence $I_t \in \mathbb{R}^{T \times H \times W \times C}$, initially set as a copy of I_s . Since the target landmark sequence L_t is generated per-landmark, we perform triangulation-based morphing, in a manner similar to Active Appearance Models [6]. This requires a common definition of N_{tri} triangles obtained with a Delaunay triangulation $\mathcal{F} = \{(l, m, n)_g \mid l, m, n \in \mathbb{N}, 1 \leq l, m, n \leq N_{ld}\}_{g=1}^{N_{tri}}$, which contains landmark index triplets.

Then, for each frame in the sequence and each index triplet $f \in \mathcal{F}$, we first calculate the affine transformation that converts the pixel coordinates of the triangle defined in the source landmarks, $\mathbf{x}_s \in \mathbb{R}^{3 \times 2}$, to its corresponding triangle in the target landmarks, $\mathbf{x}_t \in \mathbb{R}^{3 \times 2}$, and apply this transformation to the input frame:

$$I'_f = \text{Affine}(I_s^i, \mathbf{x}_s, \mathbf{x}_t), \quad (6)$$

where I_s^i is the i -th frame in I_s and $\mathbf{x}_\alpha = \{L_\alpha(j) \mid j \in \mathbf{f}\}$, $\alpha \in \{s, t\}$. Finally, we generate a blending mask M_f defined by the coordinates of the target triangle \mathbf{x}_t from the landmark indices in f , and update the target frame with a blending operation:

$$I_t^i = I_t^i \odot (1 - \sum_{f \in \mathcal{F}} M_f) + \sum_{f \in \mathcal{F}} (I'_f \odot M_f). \quad (7)$$

Algorithm 1 computes Eq. 7 but updates I_t^i with each triangle f iteratively.

The final frame sequence I_t contains temporal artifacts introduced by the LPN, which are complementary to the spatial artifacts introduced by SBI [29], when uniformly applied to all frames in a video clip with the same parameters (i.e., $\sum \|\Delta_t\|_1 = 0$, as per Eq. 2). For this reason, we can combine the two pseudo-fake generation techniques to train a network to learn both spatial and temporal clues. Furthermore, training the network with samples containing pure spatial or temporal artifacts (as opposed to mixing the two categories in the same video clip), alleviates the complexity imbalance of temporal clues during training [33, 41], as spatial clues generated by face swap are usually more dominant in deepfake videos, and the network tends to ignore the more complex temporal clues.

4 Experiments

Datasets. Following the standard practice in the literature, we use FaceForensics++ (FF++) [27] as the training dataset. It consists of 1,000 real and 4,000 fake videos constructed using 4 manipulation methods. Similar to [16, 17, 23, 29], we discard the original fake videos and use only pseudo-fake samples to train the network. The dataset provides 3

compression quality settings: raw, light compression (c23) and heavy compression (c40). As established by the literature, we employ the c23 subset, also denoted as HQ (high-quality) on other papers.

For cross-dataset evaluation, we use 5 datasets: Celeb-DFv2 (CDF) [18] (518 test videos), DFD [26] (3,431 test videos), DFDCP [8] (780 test videos), WildDeepFake (WDF) [43] (806 test videos) and DeeperForensics-1.0 (DFo) [13] (280 test videos). For further comparison, we also employ the recently released DF40 dataset [37], which contains videos from the test subset of FF++ manipulated with state-of-the-art (SOTA) deepfake generation methods. Following [23], we use the BlendFace, FSGAN and MobileSwap subsets.

Evaluation metrics. To compare our method with other SOTA deepfake detectors, we report video-level Area Under the Receiver-operating Characteristic Curve (AUC), by averaging the predictions of the network over all non-overlapping clips in a video sequence. We also provide Equal Error Rate (EER) metrics in Tab. 5 for further understanding of our results.

Implementation details. We use RetinaFace [7] to extract bounding boxes and SPIGA [24] for $N_{ld} = 68$ landmark annotations. We also align the center of the bounding box with the tip of the nose for each frame. As the deepfake detection network, we fine-tune a pretrained MARLIN encoder [2], adding an extra classification token for the deepfake detection task. The network receives sequences of $T = 16$ consecutive $224 \times 224 \times 3$ frames and outputs classification logits, which are compared to the ground-truth labels with a binary cross-entropy loss function. We follow [29] to construct batches containing real and pseudo-fake samples, but randomly choose either spatial or temporal pseudo-fakes for each sample. The data augmentation pipeline includes clip-level horizontal flip, chromatic manipulations, gaussian blur, JPEG compression, pixel dropout, affine transformations and random cropping. We use Adam optimization [15] to train the network for around 300 epochs with a maximum learning rate of $7 \cdot 10^{-6}$ and a cosine annealing scheduler with linear warm-up for the first 30 epochs. We select the model checkpoint with the lowest average loss on the validation subset of FF++, consisting of real videos and the same pseudo-fake generation methods used in the train subset. For LPN, we set $\sigma = 0.007$ as the standard deviation of the Gaussian noise, and $k = 64$ deformation bases.

4.1 Cross-dataset evaluation

Tab. 1 shows a comparison of our approach with other SOTA deepfake detection methods. Our results correspond to a ViT-L MARLIN encoder trained with a combination of spatial and our proposed temporal pseudo-fakes. As we can

Table 1. Comparison with SOTA methods in terms of video-level AUC (%). “Pristine only” refers to methods that train exclusively with pseudo-fakes. Results marked with † are computed by us with inference code and model weights provided by the authors. Otherwise, results are cited from [5, 38, 39] or from their original papers. Methods marked with * employ test-time data to select the best model checkpoint during training.

Method	Pristine only	Cross-dataset						DF40			
		CDF	DFD	DFDCP	WDF	DFo	Avg.	BlendFace	FSGAN	MobileSwap	Avg.
F3Net [25]	✗	78.90	84.40	74.90	72.80	73.00	76.80	80.80	84.50	86.70	84.00
SPSL [21]	✗	79.90	87.10	77.00	70.20	72.30	77.30	74.80	81.20	88.50	81.50
RECCE [3]	✗	82.30	89.10	73.40	75.60	78.40	79.76	83.20	94.90	92.50	90.20
SLADD [4]	✗	83.70	90.40	75.60	69.00	80.00	79.74	88.20	94.30	95.40	92.63
UCF [35]	✗	83.70	86.70	77.00	77.40	80.80	81.12	82.70	93.70	95.00	90.47
SRM [22]	✗	84.00	88.50	72.80	70.20	72.20	77.54	70.40	77.20	77.90	75.17
Altfreezing [33]	✗	89.50	98.50	70.91	59.58 †	99.30	83.56	95.10	95.80	85.10	92.00
SFA [5]	✗	89.52	86.74 †	80.58	73.70 †	99.24	85.96	-	-	-	-
PTF [14]	✗	89.70	97.30	-	-	99.40	-	-	-	-	-
LSDA [36] *	✗	89.80	95.60	81.20	75.60	89.20	86.28	87.50	93.90	93.00	91.47
FSFM [32]	✗	91.44	-	89.71	86.96	-	-	-	-	-	-
FakeRadar [19]	✗	91.70	96.20	88.50	-	-	-	-	-	-	-
CDFA [20]	✗	93.80	95.40	88.10	79.60	97.30	90.84	75.60	94.20	82.30	84.03
FCG [12]	✗	95.00	93.00 †	86.59 †	87.20	99.60	92.28	-	-	-	-
Effort [38] *	✗	95.60	96.50	90.90	84.80	97.70	93.10	87.30	95.70	95.30	92.77
SeeABLE [16]	✓	87.30	-	86.30	-	-	-	-	-	-	-
DeepShield [1]	✓	92.20	96.10	93.20	-	-	-	-	-	-	-
FakeSTormer [23]	✓	92.80	98.60	90.20	75.30	-	-	91.10	96.40	95.00	94.17
SBI (c23) [29]	✓	92.87	98.16	85.51	73.56 †	84.36 †	86.90	89.10	80.30	95.20	88.20
VB [39] *	✓	94.70	96.50	90.90	84.80	99.10	93.20	90.60	96.40	94.60	93.87
KiMoI (ours)	✓	94.74	97.04	93.89	83.52	98.47	93.53	98.06	98.05	96.86	97.66

see, our method achieves the highest average AUC, and sets a new SOTA result on DFDCP. On DF40, we achieve SOTA results on all subsets, yielding an average improvement of more than 3 points and demonstrating the generalization capabilities of our approach to a diverse range of SOTA deepfake generation techniques. The lowest AUC result for our model corresponds to the WDF dataset [43]. Note that this dataset provides pre-processed face crops instead of raw videos, which results in an extra performance drop, as our pre-processing pipeline is different. Nevertheless, our network demonstrates competitive performance even under different pre-processing variations, and surpasses methods that require deepfake videos from FF++ in combination with pseudo-fake samples [4, 20, 33]. It is also worth noting that we achieve the best generalization results without using any special network architecture or complicated multi-task framework optimized for deepfake detection, as other methods [12, 23, 39]. Existing approaches in the literature can be easily combined with our training data to achieve further improvements.

Note also that some methods [36, 38, 39] use metrics computed from test datasets to select the best performing model following the *DeepfakeBench* codebase*, which yields over-optimistic results. Still, we also surpass their results despite using videos from the FF++ validation subset to perform the model selection.

*<https://github.com/SCLBD/DeepfakeBench>

Table 2. Video-level AUC (%) obtained with different combinations of pseudo-fake generation methods. First row shows the results of a baseline model trained with original fakes from FF++ [27].

Spatial	Temporal	CDF	DFD	DFDCP	WDF	DFo	Avg.
✗	✗	85.16	87.70	79.44	72.63	99.18	87.30
✓	✗	93.75	87.32	91.34	81.76	75.12	85.77
✗	✓	64.76	99.13	76.63	72.15	98.21	82.18
✓	✓	90.10	97.05	90.84	81.80	97.79	91.52

4.2 Ablation analysis

Here we report the results obtained with the ViT-B configuration for the MARLIN encoder, unless otherwise specified. **Combination of spatial and temporal pseudo-fakes.** Tab. 2 shows the results of the network trained with different combinations of pseudo-fake generation techniques. The first row shows the results of a baseline model trained on the original fake videos from FF++. Then, we can see how a model trained on individual pseudo-fake generation techniques (i.e., spatial or temporal) only performs adequately on a subset of testing datasets, but achieves a worse average result compared to the baseline, as the network is only aware of a particular manipulation modality. However, when we combine spatial and temporal pseudo-fakes, we obtain the model with the best generalization performance, increasing the average AUC score from the baseline model by more than 4 points.

These results also showcase the different degrees of spatial and temporal clues introduced by each dataset. For

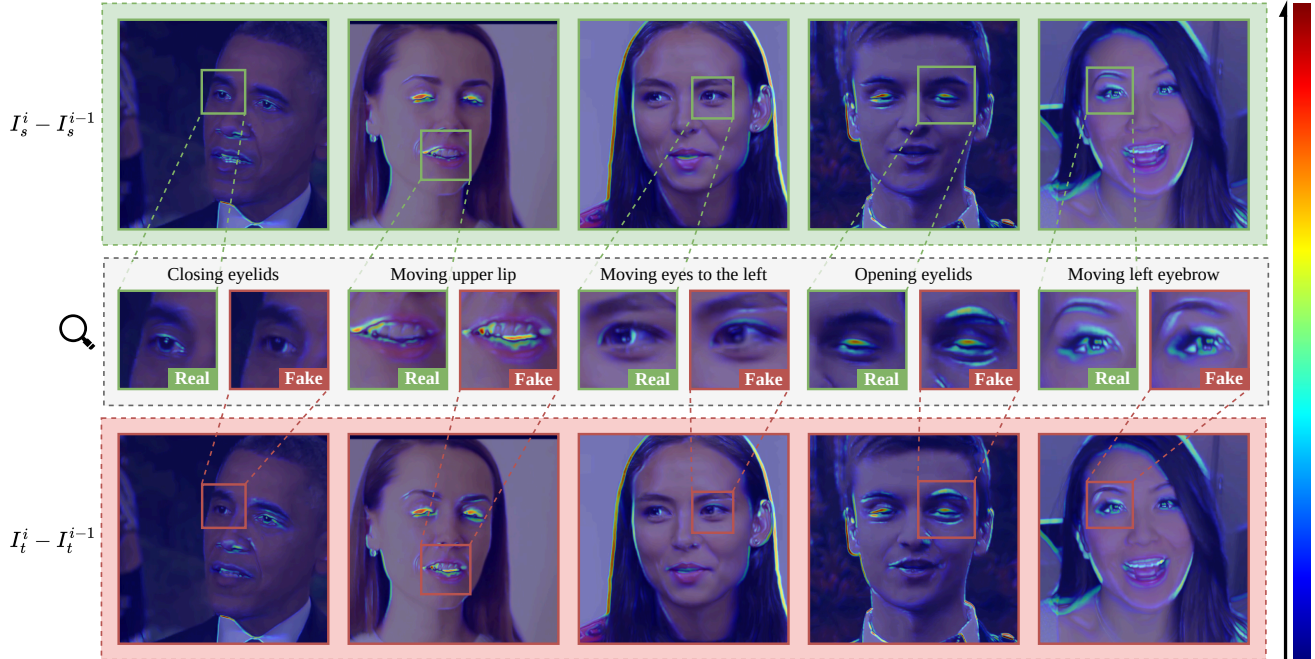


Figure 4. Visualization of subtle temporal artifacts introduced by our method (bottom row) compared to the facial movement of the corresponding real sequence (top row), extracted from pristine videos of the FF++ dataset [27].

Table 3. Comparison between different approaches for introducing temporal artifacts. All networks are trained with a combination of spatial and temporal artifacts.

Temporal artifacts	CDF	DFD	DFDCP	WDF	DFo	Avg.
Spatial baseline	93.75	87.32	91.34	81.76	75.12	85.77
Noise (iid)	93.19	91.04	88.21	81.18	88.43	88.41
Noise (multivariate)	93.98	90.61	90.88	83.16	87.46	89.22
LPN	90.10	97.05	90.84	81.80	97.79	91.52

example, we can see how fake videos in CDF or DFDCP can be easily identified by their spatial artifacts, but videos in DFD or DFo are more dominated by temporal artifacts. In particular, we achieve a SOTA result of 99.13% AUC on DFD when training only with our proposed temporal pseudo-fake samples.

Comparison between different methods for introducing temporal artifacts. To validate the importance of the LPN, we test other analytical approaches by directly manipulating landmark coordinates with subtle Gaussian noise. We designed two variants: noise sampled independently for each landmark, and multivariate noise that considers the correlation between different facial regions in temporal artifacts caused by deepfake videos (as shown in Fig. 5a). The manipulated sequence then undergoes the usual region sampling and face morphing modules depicted in Fig. 2. Tab. 3 shows the results of the network trained on a combination of spatial artifacts and this modified version of our method.

As the results show, the best generalization performance is achieved when we use the LPN, demonstrating that the artifacts introduced by the network are more semantically rich and essential to reliably identify deepfake videos. As shown in Tab. 2, DFD and DFo are the datasets that better represent the importance of temporal pseudo-fakes, as spatial clues are not as useful as in other datasets for our video-level detector. When we use our network to generate temporal artifacts, we improve the AUC results by 7 points on DFD and 9 points on DFo compared to the alternative simple and multivariate noise-based approaches.

Furthermore, we show several examples of the temporal artifacts introduced by our method in Fig. 4. Not only does it generate new movements not present in the original videos, but it is also able to introduce kinematic inconsistencies in a manner similar to the example shown in Fig. 1, as exemplified in the first and third columns of Fig. 4. To the best of our knowledge, this phenomenon cannot be reproduced by any approach in the current literature.

Comparison with other video-level pseudo-fake generation methods. Tab. 4 shows a comparison of our method with other SOTA pseudo-fake video generators, in combination with spatial artifacts. On average, our method is able to introduce more generalizable temporal artifacts.

CBI [33] is prone to introduce unrealistic temporal artifacts, yielding poor results on datasets oriented towards this type of manipulations (e.g., DFD and DFo). VB [39] performs random affine transformations to the inner part of

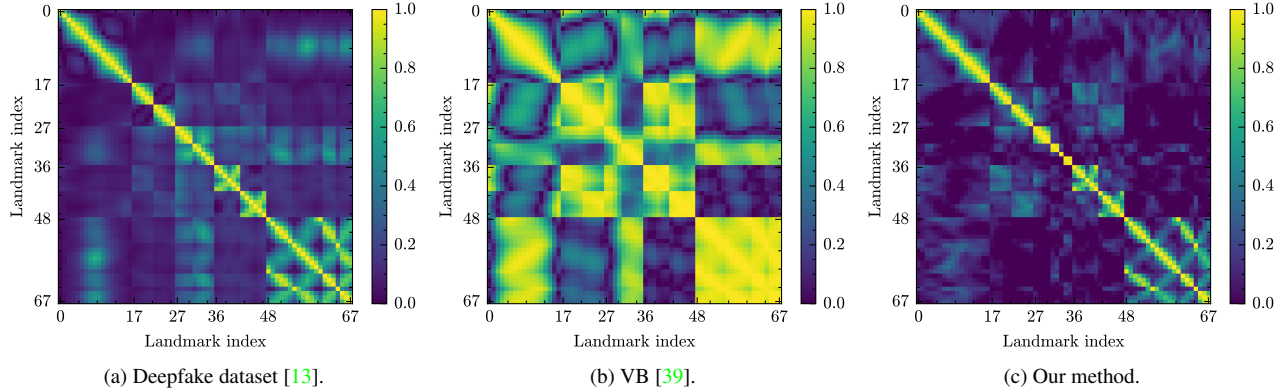


Figure 5. Correlation matrices of the temporal artifacts caused by different landmarks extracted from deepfake videos (a) and temporal pseudo-fake generators (b, c). Landmark indices correspond to the common definition of Multi-PIE [9].

Table 4. Comparison between different temporal pseudo-fake generation methods. All networks are trained with a combination of spatial and the corresponding temporal pseudo-fakes. Note that neither [33, 39] provide code, so we tested our implementation.

Method	CDF	DFD	DFDCP	WDF	DFo	Avg.
CBI (MARLIN ViT-B)	94.68	86.66	89.75	79.17	76.18	85.29
VB (MARLIN ViT-B)	91.80	95.18	87.37	82.42	95.41	90.44
KiMoI (ours)	90.10	97.05	90.84	81.80	97.79	91.52

Table 5. Video-level AUC \uparrow (% , top) and EER \downarrow (% , bottom) results for different backbone configurations of the MARLIN encoder [2].

Backbone	Parameters	CDF	DFD	DFDCP	WDF	DFo	Avg.
ViT-B	86.2M	90.10	97.05	90.84	81.80	97.79	91.52
ViT-L	303.9M	94.74	97.04	93.89	83.52	98.47	93.53
ViT-B	86.2M	17.75	9.76	18.88	27.17	6.43	16.00
ViT-L	303.9M	11.40	7.97	13.73	25.93	2.14	12.23

the face for each frame independently, which is a better approximation than the previous method, but still is not able to accurately model complex temporal artifacts, as demonstrated by the results on DFD and DFo, where our method outperforms VB by approximately 2 points.

Our data-driven approach achieves the best generalization performance and provides a flexible framework to improve the quality of pseudo-fake videos used to train the network. Furthermore, Fig. 5 shows the correlation matrices of the temporal artifacts generated by VB and our approach, compared to the correlation found on actual deepfake videos. As the figures illustrate, the correlations produced by VB exhibit a highly structured pattern. This is a direct consequence of its use of holistic affine transformations, which model facial regions as rigid units. In contrast, our approach generates a correlation matrix that more closely resembles the one produced by genuine deepfakes.

Comparison between different model sizes. To demon-

strate the scalability of our method, we train medium and large-sized versions of the MARLIN encoder, and obtain a performance improvement with the larger model across all test datasets, despite the limited size of the training dataset and the lack of regularization techniques other than data augmentation (see Tab. 5). As our approach only needs real videos to train, gathering large amounts of data to train a deepfake detection model for its use in real world scenarios becomes significantly easier, and the generic artifacts introduced by our method make the detector more resistant to overfitting to particular deepfake generation techniques.

5 Conclusions

In this paper, we presented a novel technique for generating pseudo-fake videos with subtle, generic temporal artifacts. This allowed us to train a deepfake video detection network that is not dependent on any original fake samples for its training. Empirically, it achieves a new state-of-the-art in generalization across a combination of popular deepfake detection benchmarks. We demonstrated that our synthesis approach provides more robust and transferable temporal clues than comparable methods in the literature.

The flexibility of our framework opens up future research avenues to learn interpretable deformation modes that produce semantically rich synthetic data. Furthermore, by allowing for the targeted manipulation of specific facial regions during training, we may also significantly improve the interpretability of a detector’s final decision.

In conclusion, our work establishes a new paradigm for data-driven temporal artifact synthesis, providing a robust foundation for the next generation of generalizable face forgery detection methods.

References

- [1] Yinqi Cai, Jichang Li, Zhaolun Li, Weikai Chen, Rushi Lan, Xi Xie, Xiaonan Luo, and Guanbin Li. Deepshield: Fortifying deepfake video detection with local and global forgery analysis. In *ICCV*, pages 12524–12534, 2025.
- [2] Zhixi Cai, Shreya Ghosh, Kalin Stefanov, Abhinav Dhall, Jianfei Cai, Hamid Reza Tofighi, Reza Haffari, and Munawar Hayat. MARLIN: masked autoencoder for facial video representation learning. In *CVPR*, pages 1493–1504, 2023.
- [3] Junyi Cao, Chao Ma, Taiping Yao, Shen Chen, Shouhong Ding, and Xiaokang Yang. End-to-end reconstruction-classification learning for face forgery detection. In *CVPR*, pages 4103–4112, 2022.
- [4] Liang Chen, Yong Zhang, Yibing Song, Lingqiao Liu, and Jue Wang. Self-supervised learning of adversarial example: Towards good generalizations for deepfake detection. In *CVPR*, pages 18689–18698, 2022.
- [5] Alejandro Cobo, Roberto Valle, José M. Buenaposada, and Luis Baumela. Spatiotemporal face alignment for generalizable deepfake detection. In *IEEE FG*, pages 1–6, 2025.
- [6] Timothy F. Cootes, Gareth J. Edwards, and Christopher J. Taylor. Active appearance models. *IEEE TPAMI*, 23(6):681–685, 2001.
- [7] Jiankang Deng, Jia Guo, Evangelos Ververas, Irene Kotsia, and Stefanos Zafeiriou. Retinaface: Single-shot multi-level face localisation in the wild. In *CVPR*, pages 5202–5211, 2020.
- [8] Brian Dolhansky, Russ Howes, Ben Pflaum, Nicole Baram, and Cristian Canton-Ferrer. The deepfake detection challenge (DFDC) preview dataset. *arXiv preprint*, abs/1910.08854, 2019.
- [9] Ralph Gross, Iain Matthews, Jeffrey Cohn, Takeo Kanade, and Simon Baker. Multi-pie. *Image and Vis. Comput.*, 28(5): 807–813, 2010.
- [10] Ying Guo, Cheng Zhen, and Pengfei Yan. Controllable guide-space for generalizable face forgery detection. In *ICCV*, pages 20761–20770, 2023.
- [11] Alexandros Haliassos, Rodrigo Mira, Stavros Petridis, and Maja Pantic. Leveraging real talking faces via self-supervision for robust forgery detection. In *CVPR*, pages 14930–14942, 2022.
- [12] Yue-Hua Han, Tai-Ming Huang, Kai-Lung Hua, and Jun-Cheng Chen. Towards more general video-based deepfake detection through facial component guided adaptation for foundation model. In *CVPR*, pages 22995–23005, 2025.
- [13] Liming Jiang, Ren Li, Wayne Wu, Chen Qian, and Chen Change Loy. Deepforensics-1.0: A large-scale dataset for real-world face forgery detection. In *CVPR*, pages 2886–2895, 2020.
- [14] Taehoon Kim, Jongwook Choi, Yonghyun Jeong, Haeun Noh, Jaemin Yoo, Seungryul Baek, and Jongwon Choi. Beyond spatial frequency: Pixel-wise temporal frequency-based deepfake video detection. *ICCV*, 2025.
- [15] Diederik P. Kingma and Jimmy Ba. Adam: A method for stochastic optimization. In *ICLR*, 2015.
- [16] Nicolas Larue, Ngoc-Son Vu, Vitomir Struc, Peter Peer, and Vassilis Christophides. Seeable: Soft discrepancies and bounded contrastive learning for exposing deepfakes. In *ICCV*, pages 20954–20964, 2023.
- [17] Lingzhi Li, Jianmin Bao, Ting Zhang, Hao Yang, Dong Chen, Fang Wen, and Baining Guo. Face x-ray for more general face forgery detection. In *CVPR*, pages 5000–5009, 2020.
- [18] Yuezun Li, Xin Yang, Pu Sun, Honggang Qi, and Siwei Lyu. Celeb-df: A large-scale challenging dataset for deepfake forensics. In *CVPR*, pages 3204–3213, 2020.
- [19] Zhaolun Li, Jichang Li, Yinqi Cai, Junye Chen, Xiaonan Luo, Guanbin Li, and Rushi Lan. Fakeradar: Probing forgery outliers to detect unknown deepfake videos. In *ICCV*, 2025.
- [20] Yuzhen Lin, Wentang Song, Bin Li, Yuezun Li, Jiangqun Ni, Han Chen, and Qiushi Li. Fake it till you make it: Curricular dynamic forgery augmentations towards general deepfake detection. In *ECCV*, pages 104–122, 2024.
- [21] Honggu Liu, Xiaodan Li, Wenbo Zhou, Yuefeng Chen, Yuan He, Hui Xue, Weiming Zhang, and Nenghai Yu. Spatial-phase shallow learning: Rethinking face forgery detection in frequency domain. In *CVPR*, pages 772–781, 2021.
- [22] Yuchen Luo, Yong Zhang, Junchi Yan, and Wei Liu. Generalizing face forgery detection with high-frequency features. In *CVPR*, pages 16317–16326, 2021.
- [23] Dat Nguyen, Marcella Astrid, Anis Kacem, Enjie Ghorbel, and Djamila Aouada. Vulnerability-aware spatio-temporal learning for generalizable and interpretable deepfake video detection. In *ICCV*, 2025.
- [24] Andrés Prados-Torreblanca, José Miguel Buenaposada, and Luis Baumela. Shape preserving facial landmarks with graph attention networks. In *BMVC*, 2022.
- [25] Yuyang Qian, Guojun Yin, Lu Sheng, Zixuan Chen, and Jing Shao. Thinking in frequency: Face forgery detection by mining frequency-aware clues. In *ECCV*, pages 86–103, 2020.
- [26] Google Research. Contributing data to deepfake detection research. <https://research.google/blog/contributing-data-to-deepfake-detection-research/>, 2019. Accessed: 2025-10-04.
- [27] Andreas Rössler, Davide Cozzolino, Luisa Verdoliva, Christian Riess, Justus Thies, and Matthias Nießner. Faceforensics++: Learning to detect manipulated facial images. In *ICCV*, pages 1–11, 2019.
- [28] Rui Shao, Tianxing Wu, Liqiang Nie, and Ziwei Liu. Deepfake-adaptor: Dual-level adapter for deepfake detection. *IJCV*, 133(6):3613–3628, 2025.
- [29] Kaede Shiohara and Toshihiko Yamasaki. Detecting deepfakes with self-blended images. In *CVPR*, pages 18699–18708, 2022.
- [30] Justus Thies, Michael Zollhöfer, and Matthias Nießner. Deferred neural rendering: image synthesis using neural textures. *ACM TOG*, 38(4):66:1–66:12, 2019.
- [31] Ashish Vaswani, Noam Shazeer, Niki Parmar, Jakob Uszkoreit, Llion Jones, Aidan N. Gomez, Lukasz Kaiser, and Illia Polosukhin. Attention is all you need. In *NeurIPS*, pages 5998–6008, 2017.
- [32] Gaojian Wang, Feng Lin, Tong Wu, Zhenguang Liu, Zhongjie Ba, and Kui Ren. FSFM: A generalizable face security foundation model via self-supervised facial representation learning. In *CVPR*, pages 24364–24376, 2025.

- [33] Zhendong Wang, Jianmin Bao, Wengang Zhou, Weilun Wang, and Houqiang Li. Altfreezing for more general video face forgery detection. In *CVPR*, pages 4129–4138, 2023.
- [34] Yuting Xu, Jian Liang, Gengyun Jia, Ziming Yang, Yanhao Zhang, and Ran He. TALL: thumbnail layout for deepfake video detection. In *ICCV*, pages 22601–22611, 2023.
- [35] Zhiyuan Yan, Yong Zhang, Yanbo Fan, and Baoyuan Wu. UCF: uncovering common features for generalizable deepfake detection. In *ICCV*, pages 22355–22366, 2023.
- [36] Zhiyuan Yan, Yuhao Luo, Siwei Lyu, Qingshan Liu, and Baoyuan Wu. Transcending forgery specificity with latent space augmentation for generalizable deepfake detection. In *CVPR*, pages 8984–8994, 2024.
- [37] Zhiyuan Yan, Taiping Yao, Shen Chen, Yandan Zhao, Xinghe Fu, Junwei Zhu, Donghao Luo, Chengjie Wang, Shouhong Ding, Yunsheng Wu, and Li Yuan. DF40: toward next-generation deepfake detection. In *NeurIPS*, 2024.
- [38] Zhiyuan Yan, Jiangming Wang, Peng Jin, Ke-Yue Zhang, Chengchun Liu, Shen Chen, Taiping Yao, Shouhong Ding, Baoyuan Wu, and Li Yuan. Orthogonal subspace decomposition for generalizable AI-generated image detection. In *ICML*, 2025.
- [39] Zhiyuan Yan, Yandan Zhao, Shen Chen, Mingyi Guo, Xinghe Fu, Taiping Yao, Shouhong Ding, Yunsheng Wu, and Li Yuan. Generalizing deepfake video detection with plug-and-play: Video-level blending and spatiotemporal adapter tuning. In *CVPR*, pages 12615–12625, 2025.
- [40] Hanqing Zhao, Wenbo Zhou, Dongdong Chen, Tianyi Wei, Weiming Zhang, and Nenghai Yu. Multi-attentional deepfake detection. In *CVPR*, pages 2185–2194, 2021.
- [41] Yinglin Zheng, Jianmin Bao, Dong Chen, Ming Zeng, and Fang Wen. Exploring temporal coherence for more general video face forgery detection. In *ICCV*, pages 15024–15034, 2021.
- [42] Hao Zhu, Wayne Wu, Wentao Zhu, Liming Jiang, Siwei Tang, Li Zhang, Ziwei Liu, and Chen Change Loy. Celebv-hq: A large-scale video facial attributes dataset. In *ECCV*, pages 650–667, 2022.
- [43] Bojia Zi, Minghao Chang, Jingjing Chen, Xingjun Ma, and Yu-Gang Jiang. Wilddeepfake: A challenging real-world dataset for deepfake detection. In *ACM MM*, pages 2382–2390, 2020.